Amal A. Hassan[1,*], Faten H. Fahmy[1], Abd El-Shafy A. Nafeh[1], Hosam K. M. Youssef[2]

J. Electrical Systems 18-1 (2022): 109-131

Regular paper

Control of Three-Phase Inverters for Smart Grid Integration of Photovoltaic Systems

This paper provides a smart photovoltaic (PV) inverter control strategy. The proposed controllers are the PV-side controller to track the maximum power output of the PV array and the grid-side controller to control the active and reactive power delivered to the electric grid through the inverter. A Volt-VAR regulator is proposed for controlling the reactive power exchange with the grid according to the voltage at the point of common coupling (PCC). The gains of the proposed proportional-integral (PI) controllers are optimized using a genetic algorithm (GA) via adaptive online tuning. The control methodology is then tested to a 33-bus radial distribution network under MATLAB/SimPowerSystem environment to prove the validity of the proposed control methodology and to analyze the interactions between the PV-based distributed generation (DG) and the power network. The optimal control of PV inverters demonstrated that the optimized Volt-VAR control strategy is both efficient and effective. The optimization of the PI controller parameters resulted in a good dynamic response under varying climatic conditions. The proposed control method enables the most efficient utilization of PV-DG systems by extracting maximum power and contributing to grid voltage support.

Keywords: active/reactive power control; PI controller optimization; photovoltaic grid integration; MPPT; genetic algorithm.

1. Introduction

The increasing demand for clean and reliable electricity generation from photovoltaic (PV) systems will lead to greater dependence of the grid integration requirements of these systems on advanced, efficient, and intelligent control solutions. And since the inverter is the interface unit between these renewable sources and the electric power grid, advanced control will be applied not only to generate AC power compatible with the grid power but also inverters should have some other inherent control capabilities for power management and power quality improvement to preserve the power quality regulations that imposed by the electric utility. By applying modern advanced power electronics technologies with intelligent control systems, inverters of PV systems will be more reliable, efficient, and able to control active and reactive power injected into the grid and provide dynamic grid support.

PV systems are integrated into the electric grid via voltage source converters (VSC), so it is important to control the active and reactive power and regulate the point of common coupling (PCC) voltage to avoid voltage fluctuations. The control of PV three-phase inverters for new power grids has been addressed in many pieces of research. Sarina et al. [1] presented active-reactive power control of solar photovoltaic generator with MPPT and the system was tested to a 13-bus IEEE test system. In [2], Huijuan et al. proposed a control methodology for real and reactive power for three-phase single-stage PV systems. Ansari et

* Corresponding author: Amal A. Hassan, Electronics Research Institute, Cairo, Egypt,
E-mail: amal.elramly@eri.sci.eg
[1] Electronics Research Institute, Cairo, Egypt
[2] Faculty of Engineering, Cairo University, Giza, Egypt

al. [3] provided a control methodology using fuzzy logic for MPPT of three-phase PV systems. In [4], Kim et al. presented a design and control of a grid-connected three-phase PV system using a 3-level inverter topology and LC filter. While, Saban et al. [5] focused on the MPPT of PV array using single stage, three-phase, three-level inverters. Volt-VAR control strategies were provided by Miguel et al. [6], the objective is to optimize the PV penetration into low voltage networks. In [7] Sarina et al. proposed an active-reactive power control for a two-stage PV system and the system has been tested to IEEE 13-bus system. Sotirios et al. [8] provided a control strategy for a two-stage grid-connected PV system with grid code compatibility. Many types of research such as [9][10][11] proposed a droop-based reactive power control for PV grid-connected systems. In [12], Khawla et al. discussed a control strategy for a three-phase grid-connected PV system that performs PV converter operations under normal operating conditions as well as symmetrical and asymmetrical grid voltage sag. Mohannad et al. [13] proposed a three-phase photovoltaic PID current control system tied to a low-voltage distribution grid.

In this paper, a dynamic control model of a smart grid-connected system based on a PV system is developed. The PV inverter control system consists of two control schemes which are the maximum power point tracking (MPPT) control and the power control. The objective of MPPT control is to deliver the maximum PV array power to the grid and is implemented using fuzzy logic control (FLC). The MPPT generates a reference DC-link voltage which is permitted to vary between upper and lower limits. These limits should ensure stable and safe operation of the VSC control as the generated power from the PV array is dependent on intermittent solar resources and temperature. So, FLC is used to give a proper reference voltage with minor oscillations suitable for VSC control and grid interface as will be shown later. The power control is designed to control the flow of active and reactive power into the distribution grid. This is carried out by a voltage controller and two current controllers. The voltage control is implemented to regulate the DC-link voltage to maintain the power balance between the PV array and the grid. The current control is used to control the flow of active power and to determine how much reactive power should be injected into or absorbed from the grid corresponding to the output real power and following the standards for reactive power capability of PV inverters. The IEEE 1547 standards [14][15] have recommended that DG should operate with a unity power factor (PF) or fixed PF near to unity with a maximum of ±0.95 PF operation mode. A novel optimized dynamic Volt-VAR control strategy is proposed to determine how much reactive power should be injected/absorbed for a given voltage at the PCC. The proportional-integral (PI) controllers are used to regulate the current and voltage. An integral controller is used for the Volt-VAR regulator. Adaptive online GA optimization methodology is used to optimize the PI control parameters based on three-phase d-q transformation. This paper also emphasizes the interactions between the PV system and the distribution network. Therefore, a dynamic simulation of the tested radial distribution power system is provided to reflect its performance for fast and robust analysis of the power network and to avoid the complicated mathematical model. Finally, the overall system and its proposed control methodology are implemented, tested, and verified by the simulation results implemented using the MATLAB/SimPowerSystem tool.

2. System modeling

Mathematical modeling is an essential tool to be used in the dynamic behavior and analysis of the different control strategies which will be applied to the system. Single-stage and two-stage grid-connected systems are commonly used topologies in PV applications [2]-[5]. A two-stage system has some disadvantages: less efficient, being larger, and more costly. Therefore, the single-stage structure is widely used nowadays due to its smaller size, lower cost, higher efficiency, and reliability [16].

In this paper, a single-stage three-phase multilevel inverter has been suggested to improve the performance of the proposed grid-connected PV system. Figure 1 provides the main building blocks of the three-phase grid-connected PV system. The main component of the PV system is the current-controlled VSC that interfaces the PV array with the electric grid. While Table 1 represents the design parameters of the 1 MW PV array which will be the build-up unit of the proposed system.

The PV array is connected to the DC side of VSC through a series of reverse-blocking diodes which prevent current flow from the VSC to the PV array at low solar radiation. While the AC side of the VSC is connected to the grid at the PCC through a series interface of resistance (R) and reactor (L), a shunt three-phase capacitor filter (Cf), and a three-phase transformer. The LC filter is connected in parallel to prevent the switching voltage and current harmonics generated by the PWM-based VSC from penetrating the electric grid. In emergency conditions, the circuit breaker (C.B) isolates the PV system from the distribution network. The three-phase transformer will help to set up the voltage to connect the PV system to the medium voltage distribution grid. It also acts as an isolator between the PV array system and the electric grid. In this work, the proposed PV system is considered as a distributed generation (DG) system connected to a medium voltage electric distribution grid. IEEE 33-bus test radial distribution system is utilized to test and prove the proposed control methodology. This distribution system has a total load of 3.72 MW and 2.3 MVAr at 12.66 kV voltage level [17], detailed line data and bus data of the 33-bus test system can be found at [18].

The VSC employs the pulse-width modulation (PWM) switching strategy and controls the real and reactive power delivered to the grid. Also, VSC allows the regulation of the PV array (DC) voltage and enables MPPT. The DC-link capacitor, Cdc, provides a low impedance path for the high-frequency components of the VSC DC-side current and, therefore, eliminates the DC-link voltage ripple. The control is exercised in a d-q frame that is synchronized to the grid voltage vector through a phase-locked loop (PLL) [19]. The phase-locked loop's main function is to transfer the signals from natural reference frame components (abc) to the direct and quadrature (d-q) reference synchronous frame components to perform decoupled power control and also to provide the rotation frequency at the point of common coupling (PCC). First, the PLL computes the rotation frequency of the grid voltage by transforming it to the synchronous d-q frame, and then it forces the quadrature component of the voltage (Vq) to be zero to eliminate the cross-coupling in the active and reactive powers. The d-axis component will be associated with the active power and the q-axis component with the reactive power. So the active and reactive power can be controlled with the d and q axis components as well. The rotation frequency is obtained using a proportional-integral controller. The output from the PI controller is the rotation frequency ω in rad/s. Integrating this term results in the rotation angle θ in radians.

The next sections present a detailed description of the analytical model of each component of the proposed system.

Table 1 Design parameters of 1 MW PV array

Parameter	Design value
Vdc (inverter input voltage)	600 V
Vac (inverter output voltage)	400 V
Cdc	0.1667 F
R	1.5e-4 Ω
L	50 µH
Qc	100 KVAr
The base voltage of transformer primary side	400 V
The base voltage of transformer secondary side	12.66 kV
Base Power	10 MVA

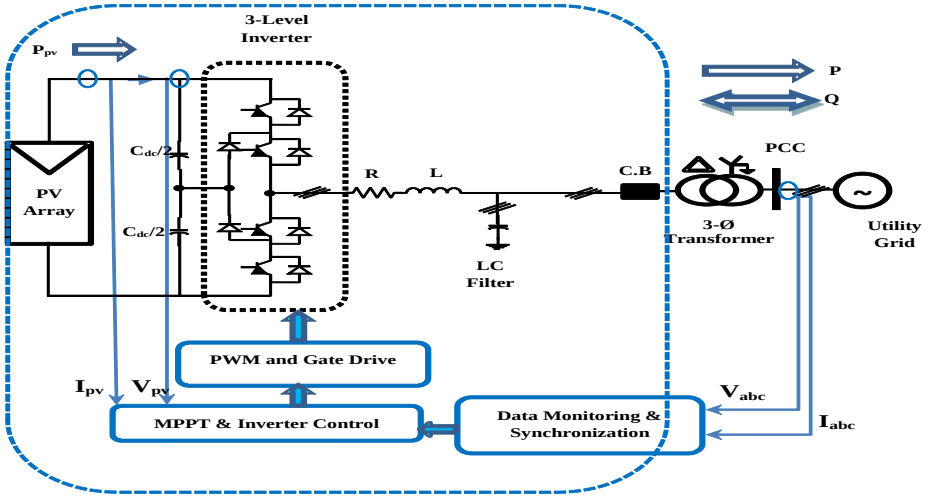

Fig. 1. Schematic diagram of single-stage/three-phase PV grid-connected system.

2.1. PV array system model

"Typically, PV cell is a simple P-N junction diode which converts solar radiation directly into electricity [20]". The PV cell model consists of a current source representing the current generated from PV, a parallel diode, shunt resistance, and series resistance. The PV array output current is represented by Eq.1 [20][21] and the technical specifications of the PV module under study are provided in Table 2.

$$i_{pv} = N_p I_l - N_p I_{os}\left(e^{(q/AkT_c)(v_{pv}/N_s + R_s i_{pv}/N_p)} - 1\right) - \frac{N_p}{R_{sh}}\left(\frac{v_{pv}}{N_s} + \frac{R_s i_{pv}}{N_p}\right) \quad (1)$$

$$I_l = \frac{Rad}{1000}\left[I_{sc} + k_{sc}\left(T_c - T_{ref}\right)\right] \quad (2)$$

Where v_{pv} is the PV module output voltage (V), N_s is the number of modules connected in series, N_p is the number of strings connected in parallel, I_l is the light generated current (A), A is the ideality factor, k is the Boltzmann's constant (1.38×10^{-23} joule/ºK), q is the electronic charge (1.602×10^{-19} coulomb), T_{ref} is the reference temperature (301ºK), I_{os} is the cell reverse saturation current (A), T_c is the cell temperature (ºC), k_{sc} is the short-circuit current temperature coefficient, *Rad* is the solar radiation (W/m^2) and I_{sc} is the module short-circuit current at 25 ºC and 1000 W/m^2.

Table 2 Technical specification of the PV module

Parameter	Value
Maximum Power (W)	260
Maximum Power Voltage Vmp (V)	31.9
Maximum Power Current Imp (A)	8.25
Open Circuit Voltage Voc (V)	37.5
Short Circuit Current Isc (A)	8.74 A
Module Area (m^2)	1.6355
Module Efficiency	15.9%

2.1. Inverter model

Voltage source inverters are mainly used to convert a constant DC voltage into 3-phase AC voltages with constant magnitude and frequency [4]. In this paper, a single-stage three-phase three-level neutral point clamped (NPC) [4][5][16] inverter will be used as an interface to transfer the PV-produced power to the grid. In this case, the inverter will carry the power conversion function and the MPPT in one stage without the requirement of other power electronic converters such as DC-DC converters as in two-stage conversion methods. The single-stage conversion with central inverter topology has the advantage of higher inverter efficiency. As efficiency is one of the major concerns in the PV system, central inverter-based PV system configuration is a better also and more economical choice. Since a single converter is used, the total harmonic distortion (THD) losses in the system are reduced. Therefore it is the first choice for medium and large-scale PV systems. The central inverter topologies are mainly built with three-phase full bridges with isolated gate bipolar transistors (IGBTs) and the low-frequency system as shown in Figure 1. The inverter is composed of twelve switches with each phase output connected to the middle of each "inverter leg". Two switches in each phase are used to construct one leg. The inverter output AC voltage is obtained by controlling the semiconductor switches ON/OFF to generate the desired output waveform. Pulse width modulation (PWM) techniques are widely used to perform this task. In which three reference signals are compared to a high-frequency carrier waveform. The result of that comparison in each leg is used to turn the switches ON or OFF. This technique is referred to as sinusoidal pulse width modulation (SPWM). It should be stated that the switches in each leg should be operated interchangeably, to avoid a short circuit of the DC supply. Insulated Gate Bipolar Transistors (IGBTs) and power MOSFET devices can be used to implement the switches.

The NPC inverter topology offers many advantages which are reduced switching losses; only half the voltage has to be switched resulting in reduced switching losses in the transistor. In the proposed system, NPC topology uses 300V components instead of 600V types. The NPC topology also has lower output voltage transients and reduced ripple in the output current. This will reduce the size and cost of the required filter for filtering and isolation functions. Another advantage is that the total +/- supply voltage is shared; the DC

voltage is divided in a positive and in a negative voltage which supports the serial connection of DC-capacitors without problems of leakage compensation.

Three-phase inverter-based PV systems are with power ratings higher than 5 kW and are usually grid-connected. Three-phase converters are practically implemented in the PV system using three single-phase converters connected to each load terminal [4][5]. This is because for a three-wire topology relatively higher DC voltage value (600 V for a 400 V three-phase grid) is required and is limited to 1000 V due to safety reasons in installation procedures [3].

3. Control of the three-phase PV inverter

A control system of a grid-connected three-phase 3-level inverter system as shown in Figure 1 consists of two main controllers; the PV-side controller for the maximum power point tracking (MPPT), and the AC-side controller for the inverter. These controllers are incorporated with the overall system controller in the inverter circuit that is regulated with the DC link voltage, the line voltage at the PCC, the inverter current, and the grid current. The PV-side controller is used to regulate the DC link voltage of the inverter; to achieve the maximum power from the PV array. FLC method is applied for the MPPT. Three PI controllers will be used for voltage and current controllers of the VSC control, while, an integral controller will be used for the Volt-VAR regulator.

The control function of the 3-level NPC inverter is to regulate DC voltage and supply power generated by the PV array to the grid with low harmonic currents. The current controller is implemented in the d-q synchronous frame and its manipulated variables are generated in the d-q coordinate system. Since phase quantities are required in the PWM switching pattern, PI controller results are transformed back to the abc coordinate system and then back into phase quantities.

3.1 PV-side controller - MPPT

The PV controller's purpose is to extract the maximum power of PV arrays considering the nature of the resource (intermittent solar radiation and temperature). There are several methodologies to track the maximum power point (MPP) of the PV array divided into two categories: conventional methods and artificial intelligence methods [22][23][24].The most famous based conventional MPPT methods are the Perturb and Observe (P&O) and the Incremental Conductance method. The artificial intelligence-based methods are Fuzzy logic-based MPPT and Neural Networks based ones. Both Conventional and artificial intelligence (AI) methods have their advantages and drawbacks. Conventional methods are easy to implement and compatible to operate with Photovoltaic array of any size, while their disadvantages are that they are considered slower than other artificial intelligence methods and they also show slow response in sudden temperature and solar irradiance changes, so they may fail in tracking the maximum power. Moreover, artificial intelligence-based MPPT methods show very fast response under any operating condition changes, resulting in very accurate results and they can work under instant temperature or solar irradiance changes efficiently. The drawbacks of the AI methods are that they are complicated in design, they need very fast processors to be implemented physically or otherwise, they will run very slowly. In our work, a conventional method P&O is compared

to the Fuzzy logic-based method. In the applied methods, the output of MPPT generates voltage reference for the inverter voltage controller.

3.1.1 The perturb and observe method

Perturb and observe (P&O) MPPT technique is the most widely used one as it is the simplest method of all MPPT techniques [22][23]. In P&O, the terminal voltage and output current of the PV array is measured, and then the actual Power can be calculated and the reference voltage output of the PV array is varied until the MPP is achieved. The drawback of the P&O algorithm is that in case of a sudden increase in solar irradiance, the P&O reacts as if the increase occurred as a result of the previous perturbation of the array operating voltage. Therefore, the next operation will be in the same direction as the previous one which may be the opposite direction of maximum power. When the irradiance change decreases or stops the MPPT will get back to its normal behavior [22][23][24].

3.1.2 Fuzzy logic-based MPPT

As mentioned earlier that in the case of grid interface, a constant DC reference must be supplied to the VSC for stable operation of PV grid-connected system. Moreover, the conventional MPPT techniques change the reference voltage in a wider range with the change of solar radiation. FLC has been used in the MPPT of PV systems especially single-stage ones as it is robust and relatively simple to design and the required output, in that case, is the voltage reference. FLC is also suitable for nonlinear problems [2][3][25]. The proposed system in this study is a single-stage; it doesn't contain a DC-DC converter. Therefore, the MPPT controller will output a DC reference voltage as an input to the inverter, not a duty cycle. The slope of the P-V curve ($\Delta P_{pv}/\Delta V_{pv}$) and the change of slope (ΔE) were used in this work as the input control variables to the fuzzification stage. The inputs to the FLC are the change in voltage and the change in the PV array output power. The FLC output will be the change in DC voltage (ΔV) which is then integrated to obtain the desired reference DC input voltage to the inverter. Seven membership functions are defined for the input variables and nine membership functions for the output variable. The shapes of these functions are triangular and they are normalized to [-1 1], [-2 2] for the input variables, and [-1 1] for the output variable. Because of normalization, the characteristics are controlled through input and output gains, to reduce the tuning complexity of the FLC.

$$E = \frac{\Delta P_{pv}}{\Delta V_{pv}} = \frac{P_{pv}(j+1) - P_{pv}(j)}{V_{pv}(j+1) - V_{pv}(j)} \tag{3}$$

$$\Delta E = E(j+1) - E(j) \tag{4}$$

Where E and ΔE are the error and change of error, respectively, ΔP_{pv} and ΔV_{pv} are the change in PV array output power and the change in PV array output voltage, respectively.

3.2 Grid-side controller

This controller has the purpose to fulfill these basic requirements: control of the active power delivered by the source to the grid, control of the reactive power exchange with the grid, power quality regulations; high quality and high efficiency of the injected power, and grid synchronization.

The grid-side controller as illustrated in Figure 2 consists of two control schemes discussed as follows:

3.2.1 The voltage controller

The DC output voltage of the PV array is measured after passing through a low pass filter to attenuate any high-frequency components and then compared to the dc voltage reference outputs from the MPPT controller to generate the d-axis current reference I_{dref}. The DC voltage regulation is implemented to control the active power output of the inverter. The equation of this control loop is given as follows [9][26]:

$$I_{dref} = k_p \times (V_{dc} - V_{dcref}) + k_i \times \int_0^t (V_{dc} - V_{dcref})dt \tag{5}$$

Where I_{dref} is the reference value of the d-axis current component, V_{dc} and V_{dcref} are the DC actual and reference value of the input voltage to the inverter (PV side). k_p and k_i are the proportional and integral gains of the PI voltage controller.

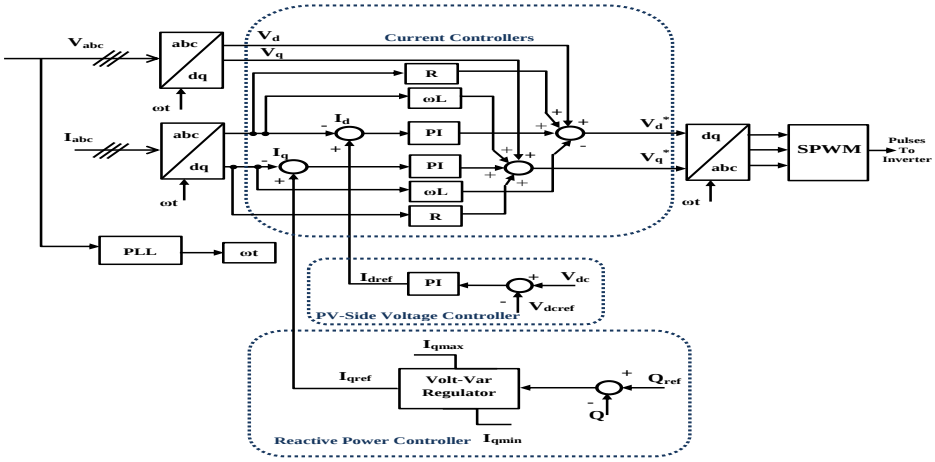

Fig. 2. Control of the three-phase VSC in the d-q frame.

3.2.2 The current controllers

The current controllers consist of two control loops for active and reactive power control. These current controllers are used to regulate the output power of the PV array system. Each current loop contains a PI controller that regulates the output current to follow its reference values. The measured three-phase voltages and currents at the PCC are transformed to the synchronously rotating reference at the grid frequency as clarified in Figure 2. Then the current reference designed with synchronous reference d-q axis frame is oriented to the d-axis rotating at the grid frequency. The output of PI controllers is used to

generate the voltage commands for the inverter PWM switching. The current control loops can be expressed in the rotating d-q reference frame by the following equations [9][26]:

$$\Delta V_d = K_{pc} \times \left(I_d - I_{dref}\right) + K_{ic} \times \int_0^t \left(I_d - I_{dref}\right) dt \quad (6)$$

$$\Delta V_q = K_{pc} \times \left(I_q - I_{qref}\right) + K_{ic} \times \int_0^t \left(I_q - I_{qref}\right) dt \quad (7)$$

$$V_d^* = R_T I_d - \omega_g L_T I_q + \Delta V_d + V_d \quad (8)$$

$$V_q^* = R_T I_q - \omega_g L_T I_d + \Delta V_q + V_q \quad (9)$$

Where, ΔV_d and ΔVq are the controlled values of the d-axis and q-axis components of PCC voltage, I_d is the d-axis actual current, respectively, I_q and I_{qref} are the q-axis actual and reference current, respectively, V_d and V_q are the d-axis and q-axis components of the PCC voltage, V_d^* and V_q^* are the reference values of d-axis and q-axis components of the PCC voltage, respectively, K_{pc} and K_{ic} are the PI gains for current controllers, R_T and L_T are the total feed-forward resistance and inductance, respectively. ω_g is the angular frequency of the grid, $\omega_g = 2\pi f$ where f is the fundamental frequency (50 Hz).

3.2.3 Reactive power control strategy

It is commonly known that PV systems provide only active power. The objective of a reactive power controller is to enable the inverter to provide reactive power in addition to the active power. Reactive power control methodologies can be static or dynamic. In static reactive power control, the amount of reactive power can be identified using a constant or a variable power factor. This method has the drawback that it may cause additional reactive power flow in the network even when the grid voltage is within the limits. Using the dynamic reactive power control, the reactive power injected into the grid can be controlled based on PCC voltage regulation. The reactive power control can be implemented using different methods:

Fixed unity power factor: In the case of unity power factor, there is no reactive power support (in that case the reference reactive power (Qref) will be zero).

Static reactive power control (fixed or variable power factor): The static reactive power control methodologies have the drawback that they may cause additional reactive power flow and may lead to overloading of the distribution transformer.

Dynamic Volt-VAR control (fixed or variable power factor): Figure 3 provides the proposed dynamic Volt-VAR regulator. The objective of this methodology is to maintain the voltage at the PCC at its steady-state limit. The grid voltage will be compared to its reference value and the voltage regulation will be achieved with the injection or absorption of reactive power according to the PV inverter's reactive power capability limit. The output of this controller is Iqref and its min and max limits can be calculated using the following formula [26][27]:

$$Q_{\max} = -\left(3/2\right) \times V_d I_q \quad (10)$$

Where Q_{max} is the maximum permissible reactive power of the PV system which corresponds to 0.95 PF; according to the allowable reactive power capability of PV inverters shown in Figure 4 [28]. According to the system operator, control system, and the method used for reactive power control, the reactive power that is to be transferred is

decided. The half-circle denotes the power capability limit of the inverter. The inverter cannot operate outside its limit since it is limited by the nominal power of the generator. For operating at 0.95 PF, the operating region is determined by the two vertical lines.

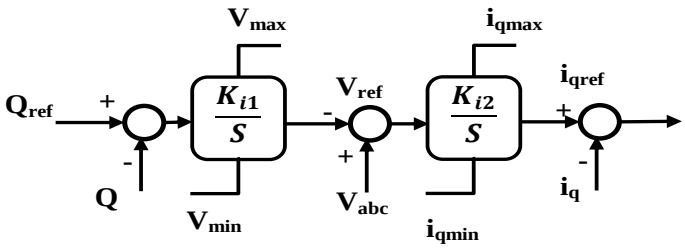

Fig. 3. Block diagram of dynamic Volt-VAR regulator.

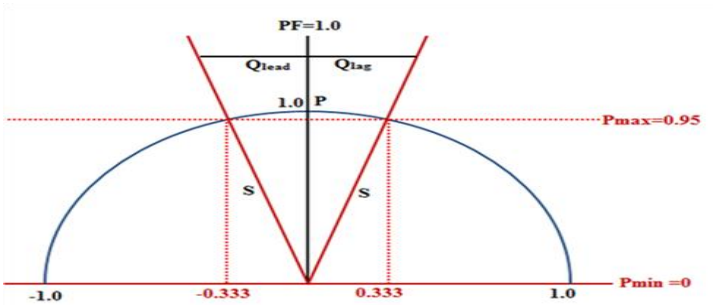

Fig. 4. Capability curve of the inverter.

4. GA-based PI controller tuning

GA optimization methodology is utilized to search the optimal parameters of the multiple PV system controllers. GA has been widely used for solving optimization problems of electrical power systems. The heuristic search of GA is based on the principle of survival of the fittest. The GA is initialized with a set of randomly generated initial candidate individuals. These individuals are subjected to a selection process based on their relative fitness. New candidate solutions are created from the previous set by genetic operators (crossover and mutation) [15][29]. To run the GA solver, it is necessary to provide the fitness function, the number of parameters, and the boundary limit of the parameters which is needed to limit the solution within the design space. Figure 5 shows the flowchart of the proposed GA optimization methodology for the PI parameters' tuning.

The voltage PI controller, current PI controllers, and Volt-VAR regulator parameters are tuned by applying a genetic algorithm (GA). The errors are measured and a fitness evaluation function is performed to calculate the overall responses for each of the sets of PI gains and from the responses generates a fitness value for each set of individuals which can be expressed by [30]:

$$f(x) = \int_0^t t|e(t)|dt \tag{11}$$

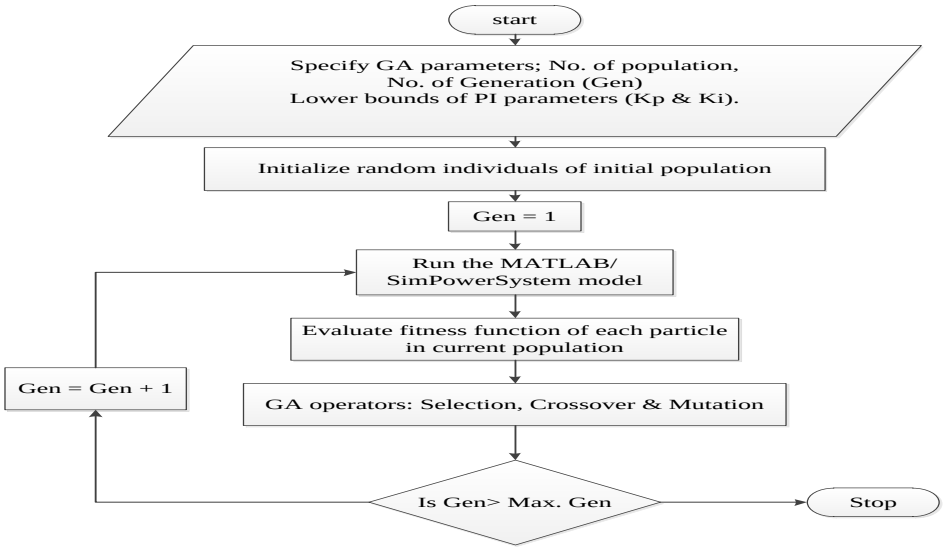

Fig. 5. Flowchart of PI tuning optimization.

The goal of the indicated objective function is to find the set of PI parameters that gives a minimum fitness value (i.e. minimum error *e(t)*) over the period [0, t]. The fitness function is the integration of time multiplied by absolute error (Integral of the time-weighted absolute error (ITEA) criterion). When this cycle is completed, it produces new sets of PI values which ideally will be at the fitness level higher than the initial population of PI values. These new sets of PI values are then passed to the fitness evaluation function again where this process is repeated until reaching the tolerance or the stop criterion is met. This process is performed by interfacing the MATLAB/SimPowerSystem and the GA optimization toolbox in the MATLAB environment through adaptive online optimization methodology. This means that the objective function value and gain values are assigned during the execution of the program which allows the PI gains to be updated while the simulation is running until reaching the optimal gain values (achieve the objective function and fulfill the system's constraints).

5. System simulation

A simulation of the 33-bus radial test system is conducted in MATLAB/SimPowerSystem toolbox to demonstrate the effectiveness of the developed smart inverter control system. The simulation time is adjusted to run for 1.5 seconds with a sampling period of 5µs. The dynamic modeling of the power system with the installed renewable energy systems is very important to test the dynamic behavior of the complete system. Also, it is very important to test the radial system with renewable energy using realistic data of solar radiation and analyzing the control system performance. The real-time simulation is also important for checking the improvement in energy losses and investigating the voltage profiles under various meteorological conditions. Figures 6-8 show the implementation of the three-phase PV-based DG connected to a 33-bus radial power system. The figures also represent the implementation of different control systems

for Fuzzy-MPPT and VSC. Energy management and monitoring unit are used for monitoring and three-phase measurements of the whole parameters of the proposed and tested systems, then calculating the power flow and obtaining the voltages at all buses and power losses at all branches using variable solar radiation data. The capacities of PV arrays are optimally achieved as indicated in [31]. The optimal PV array sizes are 800 kW and 1 MW located at buses 14 and 30. The total number of series modules N_s is determined according to the operating system voltage (600 V), which will be 19. While the total number of parallel strings N_p is depending on the rated power of the PV array and the number of series modules. For an 800 kW PV system, N_p is 164, while in the case of a 1 MW PV system, N_p is 205.

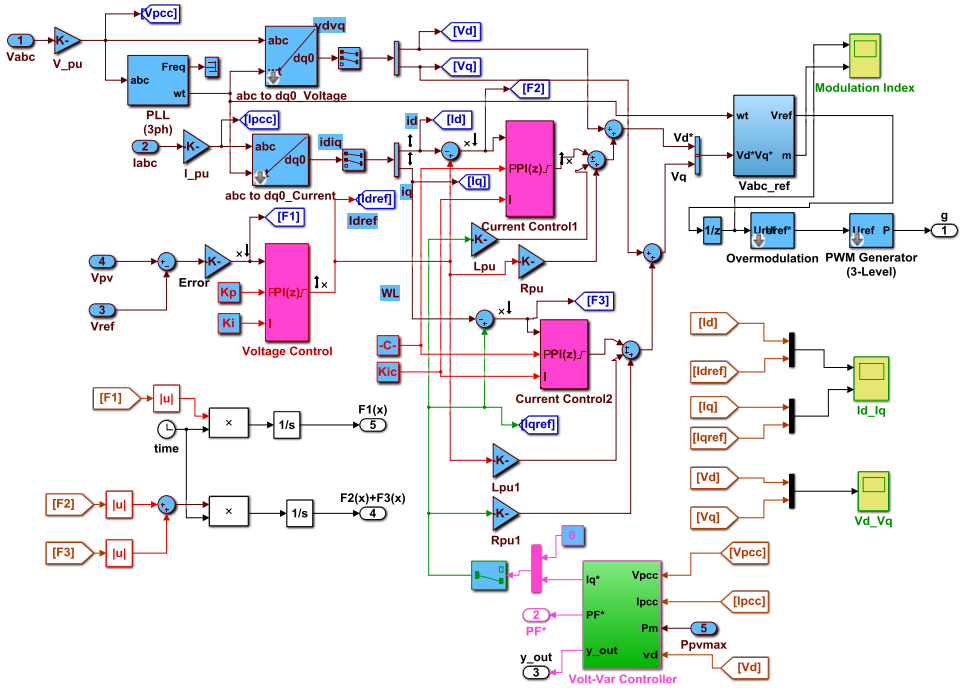

Fig. 6. Implementation of VSC voltage and current controllers in MATLAB/SIMULINK.

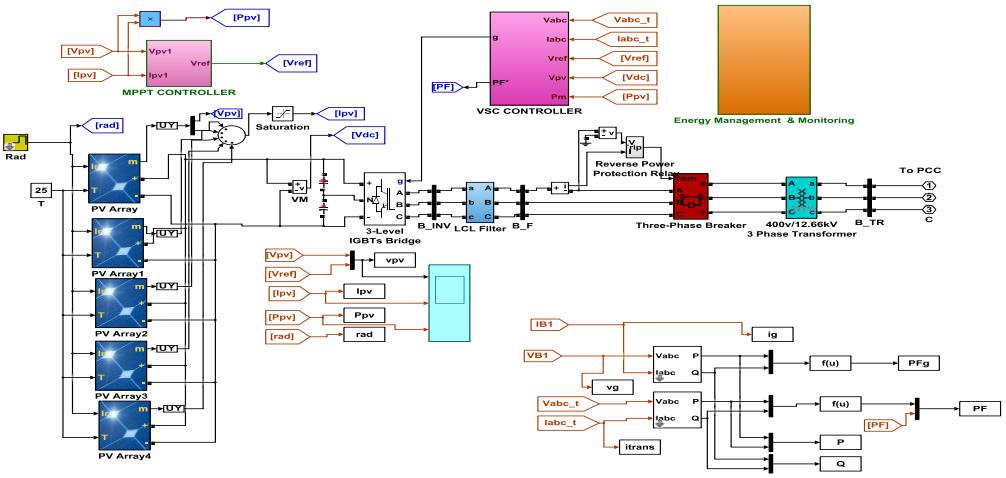

Fig. 7. Implementation of 1 MW PV array system in MATLAB/SIMULINK.

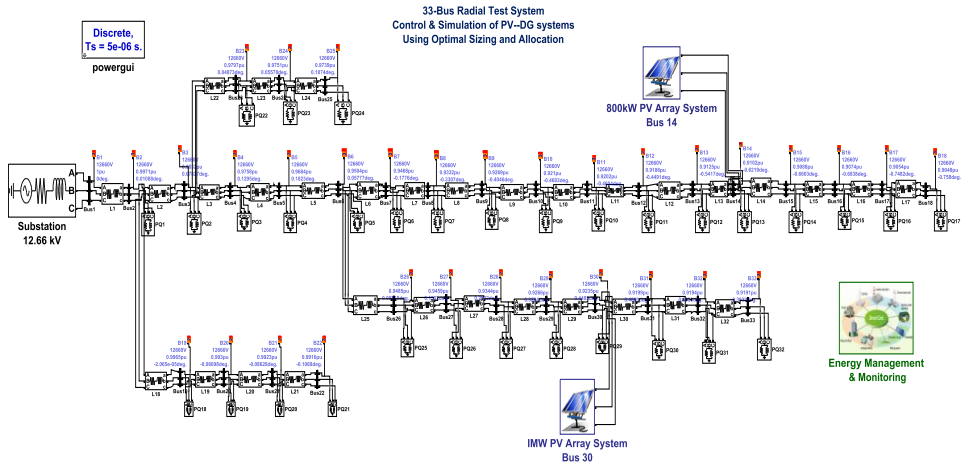

Fig. 8. Implementation of PV array connected to the 33-bus radial test system in MATLAB/SIMULINK.

6. Results and discussion

The dynamic modeling of the PV array system is implemented in the MATLAB/SimPowerSystem toolbox to verify the system performance and test the applied control methodology. The test is done under various scenarios using practical data for the tested power system, real weather data for solar radiation and temperature.

Figure 9 shows the maximum output power of the PV array for different MPPT techniques; P&O and the proposed fuzzy method at different radiation levels. The fuzzy method gives better results for transient and steady-state operating conditions of the PV array. It is clear also that the output power is proportional to the solar radiation. Thus, FLC can perform MPPT effectively under changing weather conditions.

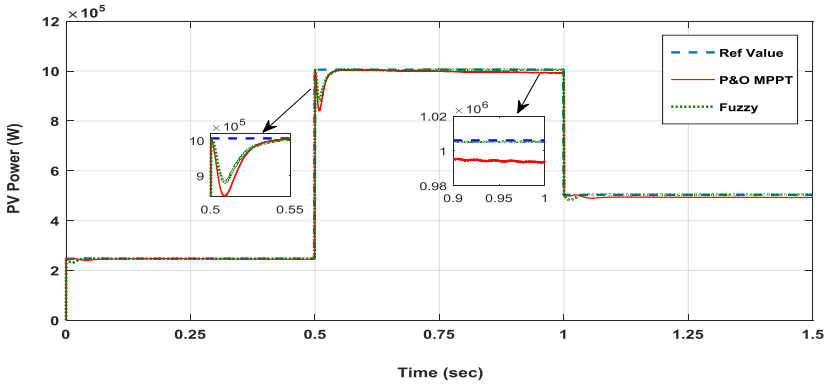

Fig. 9. The maximum output power of PV array for different MPPT techniques.

6.1 Optimal PI tuning using GA

Table 3 represents the optimal tuned parameters of the PV system's PI controllers using GA. While Figure 10 clarifies the fitness function convergence of the voltage controller. Figures 11 and 12 give the fitness function convergence of current and Volt-VAR controllers, respectively. As shown in these figures, the fitness function value of the error decreases until reaching the best fitness value after approximately ten generations. The GA stops at generation 41 before reaching the maximum number of generations (50) as the error tolerance is achieved and minimized to the best value. The effect of tuned parameters on the overall system's performance will be discussed in the following sections.

Table 3 Tuned parameters of PI controllers using GA

PI controller	Kp	Ki
Voltage controller	1.25	379.836
Current controllers	0.559	24.757
Var controller	------	127.8

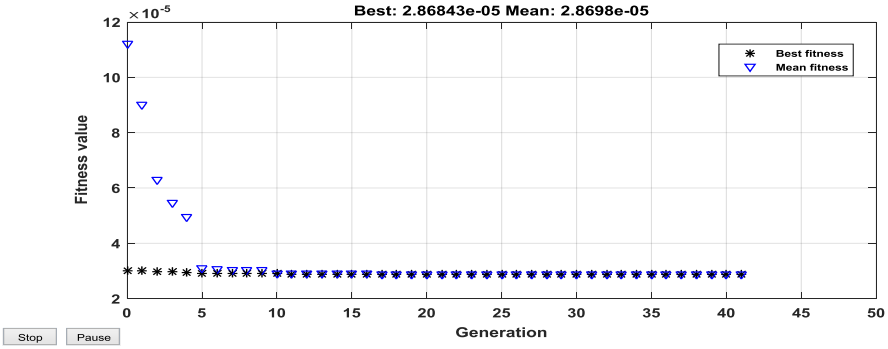

Fig. 10. Convergence of voltage controller's fitness function.

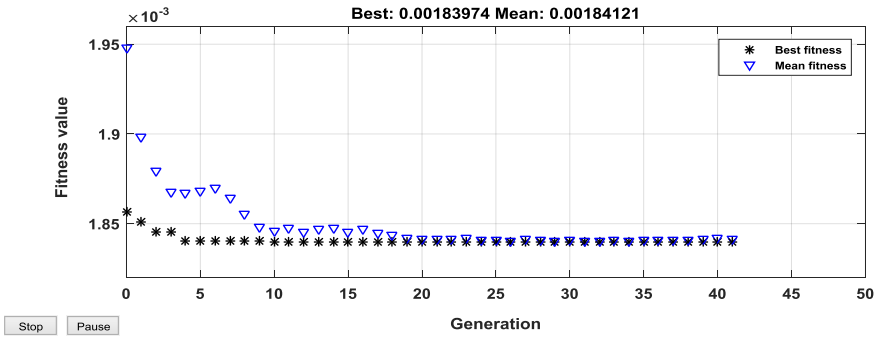

Fig. 11. Convergence of current controller's fitness function.

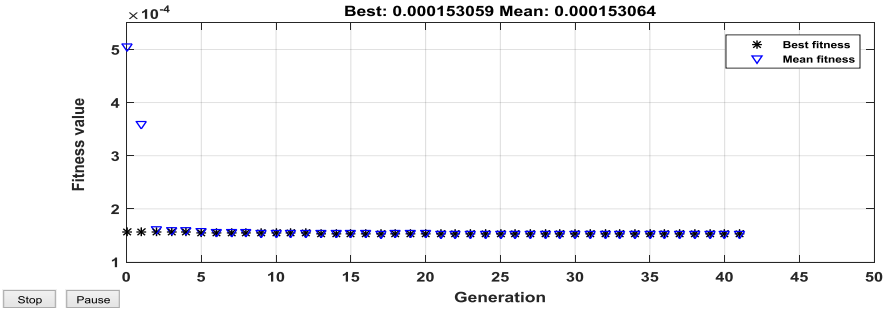

Fig. 12. Convergence of volt-var controller's fitness function.

6.2 Unity PF operation mode

The inverter was controlled at two operating modes: Unity PF and the reactive power generation mode at which the voltage is regulated by controlling the supplied reactive power. In that case, the PF is adjusted to be 0.95 to be able to deliver reactive power to the power system within the accepted grid limits. Figure 13 shows the PV array output voltage against the reference voltage generated by the MPPT controller with and without tuning, it is clear from this figure that the fuzzy-based MPPT control system finds the best possible DC voltage output that ensures the maximum power point of the PV array and at the same time maintaining the DC voltage stability which is very important to single-stage inverters with Volt-VAR control function.

Figures 14 and 15 illustrate the d-q components of PCC current against the reference values of I_d and I_q generated from the two PI current controllers before and after optimal tuning. Regardless of the operating point of the PV system, the power factor is adjusted to be unity (Qref = 0), so the Iq is equal to zero. Therefore, the PV system supplies no reactive power with the help of optimally tuned current controllers; there will not be any regulation over the AC voltage. I_d is the current component that is responsible for controlling the active power output of the inverter delivered to the electric grid at PCC. Therefore, it can be observed that I_d changes linearly according to the solar radiation level. It can be depicted also that with GA tuning, there is an effective change of I_d towards the optimal reference value. GA tuning results in a better dynamic response of the PI controllers and therefore they give a better dynamic performance of the whole system.

For the voltage at the PCC, the PLL forced the quadrature component of the voltage (V_q) to be zero to decouple the active and reactive power control. The d-axis component will be associated with the active power and the q-axis component with the reactive power. The maximum value of the output AC voltage is 400 V corresponding to 600 DC input voltage as discussed earlier. The total harmonic distortion (THD) in the output AC waveforms is calculated using the fast Fourier transform (FFT) toolbox in MATLAB/SimPowerSystem. The THD in the inverter output voltage waveform is 40.64% reduced to the standard limits after passing the LC filter.

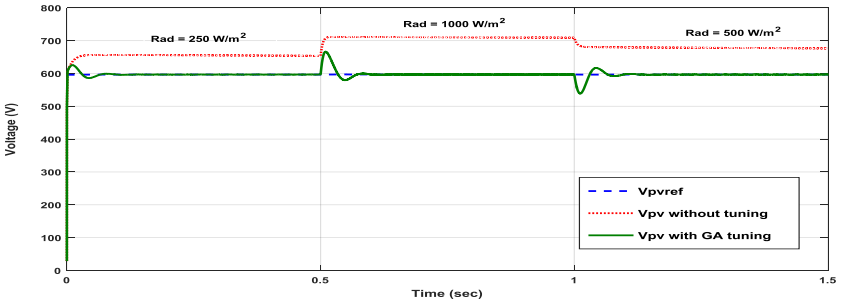

Fig. 13. The PV array output voltage at different radiation levels.

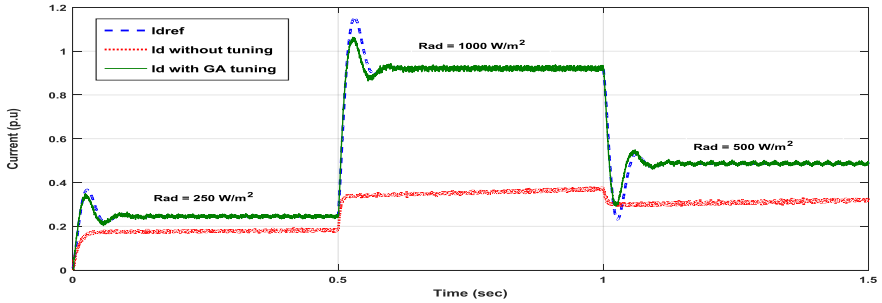

Fig. 14. Actual and reference direct control currents.

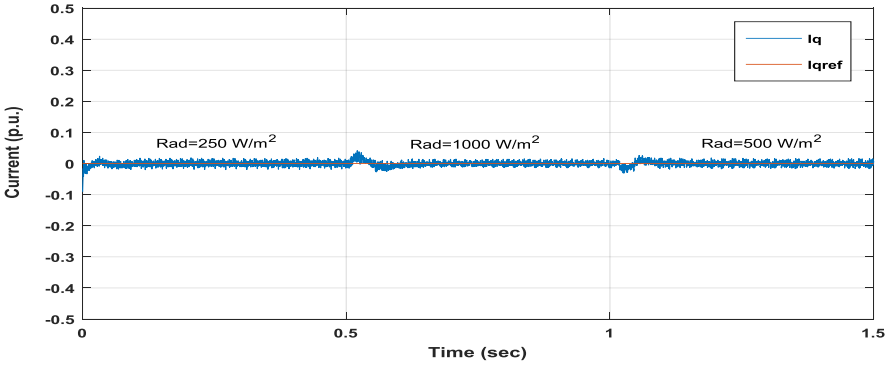

Fig. 15. Actual and reference quadrature control currents.

The output voltage of the LC filter is almost pure sine. The THD in the filtered voltage waveform is 4.07% during transients (regarding that the simulation is performed under the high transition of solar radiation – it is changing from 250 W/m2 to 1000 W/m2). While,

the THD at steady-state conditions is approximately 1.33% representing a very good waveform; delivering power of high quality to the electric distribution system. The PV output AC voltage is 400 V and the voltage level of the tested 33-bus system is 12.66 kV, so, a transformer is required for voltage boosting and isolation of the PV system and the electric grid. The THD in the transformer secondary voltage waveform is 1.29% during radiation change periods and 0.36% during steady-state conditions.

Figure 16 shows the current at PCC of the PV array and the current drawn from the substation. At a low radiation level, the AC output current of the PV array is low, so, more current will be drawn from the electric grid to supply the electric loads. At a high radiation level (1000 W/m2), the current drawn from the electric grid will decrease as the PV array output current increases.

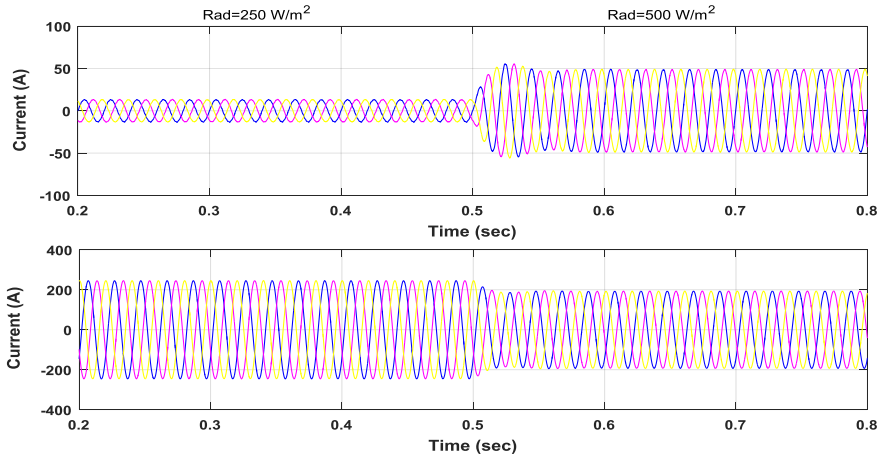

Fig. 16. Current waveforms at different points of the system.

Figure 17 provides the PV array output power delivered to the electric grid at PCC, the total load power (active and reactive), and the power supplied from the electric grid of the 33-bus test system. It can be depicted from this figure that the load is fed from the substation and the PV generating units. Therefore, the power supplied from the grid will decrease as the PV array output power increases. It can also be noticed from the figure that the maximum value of PV array power changes according to the solar radiation based on a linear relationship that exists between solar radiation and PV array output power. It is also clear that the MPPT based FLC tracks the maximum output power of the PV array. The tested system consists of two PV array systems rated 800 kW and 1 MW placed at buses 14 and 30, respectively. The total active power load of this system is 3.72 MW and the total maximum output power of the PV arrays at the standard radiation level (1000 W/m2) is 1.8 MW. Figure 18 shows the reactive power, the output reactive power of PV inverter remains zero irrespective of the radiation change keeping the power factor unity. Therefore, the reactive load is supplied from the electric grid. In that case, the substation power is feeding the electric loads and the total system losses.

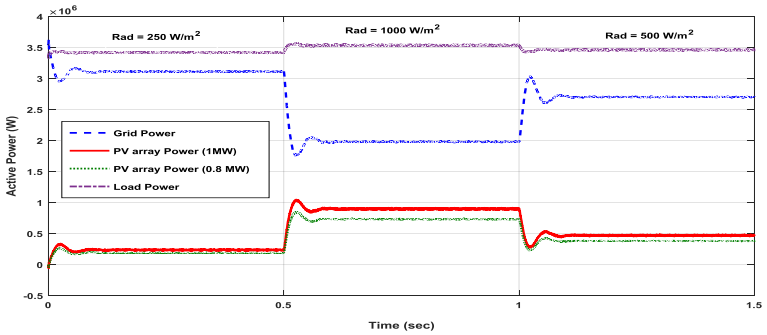

Fig. 17. PV array output power, load power, and grid power for the 33-bus system.

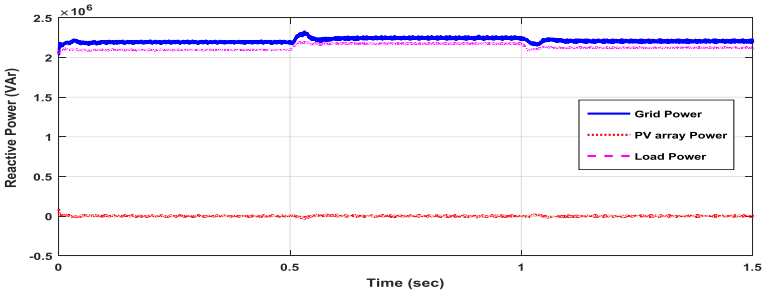

Fig. 18. Reactive PV array output power,load power, and grid power for the 33-bus system.

The AC voltage regulation tries to keep the voltage at PCC at a certain defined level through the Volt-VAR controller which provides sufficient reactive power according to the inverter reactive power capability curve limits. Figure 19 represents the quadrature current component responsible for reactive power exchange pre and post-tuning of the Volt-VAR regulator at different radiation levels. The Volt-VAR controller operates to control the reactive power exchange at the PCC to regulate the voltage within the standard limits. It can be depicted also that with GA tuning, there is a better dynamic response of the Volt-VAR controller. The regulator also gives better tracking of the Iq optimal reference value. The Volt-VAR controller is tested for two cases: dynamic reactive power control using variable PF and fixed PF (0.95 lag and lead). In the case of variable PF, the inverter capability according to Figure 7 is the circle diameter. While in the case of fixed PF, the reactive power capability of the inverter is between -0.333 and 0.333 p.u to preserve the PF limits within 0.95 lead or lag.

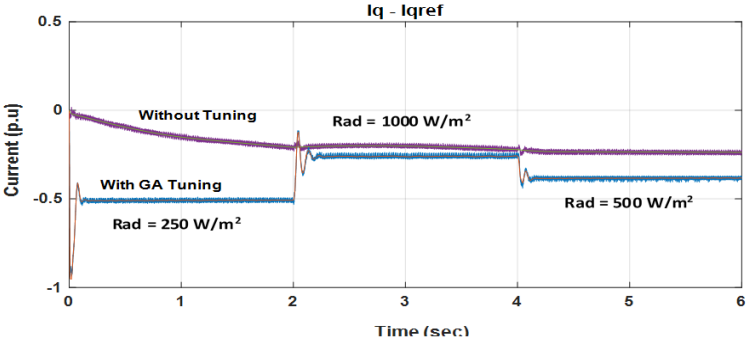

Fig. 19. Quadrature current component with and without tuning of Volt-VAR regulator.

Figure 20 clarifies the quadrature current for different loads (resistive, inductive, and capacitive) with dynamic Volt-VAR control at variable PF. If Iq is greater than zero, then

the inverter absorbs reactive power. But, if the value of Iq is less than zero, then the inverter delivers reactive power to the power system. In that case, the voltage magnitude at the PCC will be constant regardless of the load change and solar radiation change as illustrated in Figure 21. The AC voltage regulator keeps the voltage at the PCC at a certain defined level.

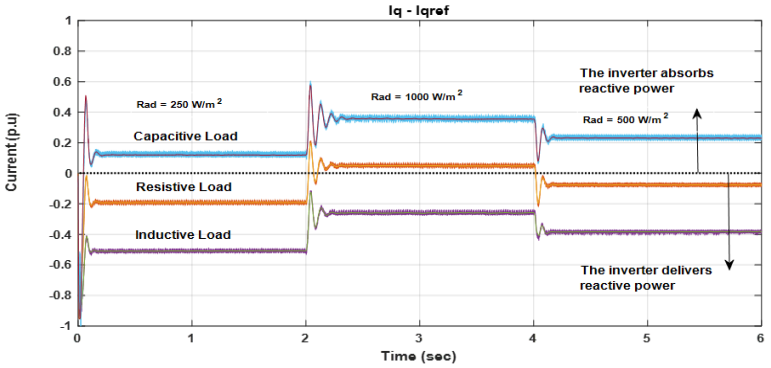

Fig. 20. Quadrature current for different loads with dynamic Volt-VAR control at variable PF.

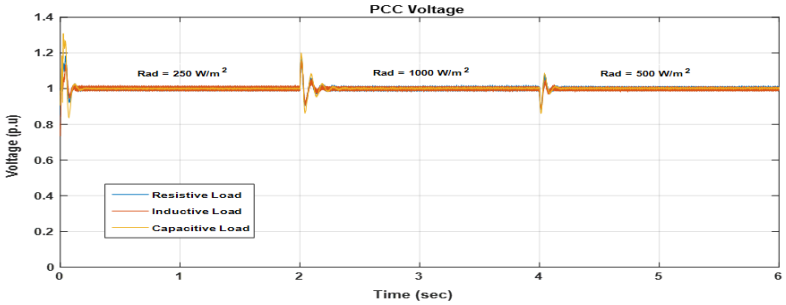

Fig. 21. The voltage at PCC for different loads with dynamic Volt-VAR control at variable PF.

Figure 22 represents the quadrature current for different loads with dynamic Volt-VAR control at fixed PF. It can be noted that the actual current and the reference current curves coincide which means that the Volt-VAR controller tracks the reference current value. While Figure 23 shows the PCC voltage for the same case. It can be depicted that the reactive power exchange is less than its value in the case of variable PF as it has been restricted to the standard reactive power capability curve for the PV inverter (As noted in Figure 6, the Q compensation is restricted to the two vertical lines ±0.33 for 0.95 PF lag or lead). It can be noted also that the PCC voltage is changing but within the allowable limits, especially at high radiation levels.

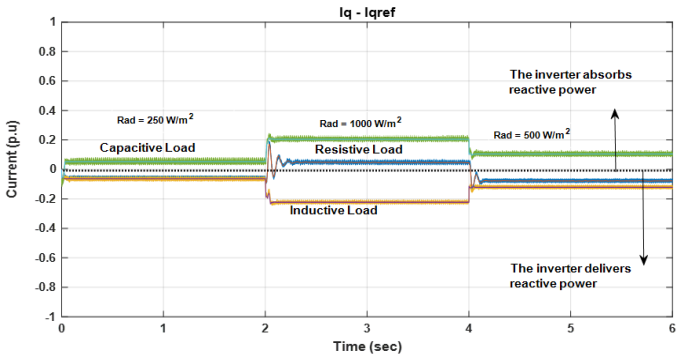

Fig. 22. Quadrature current for different loads with dynamic Volt-VAR control at fixed PF.

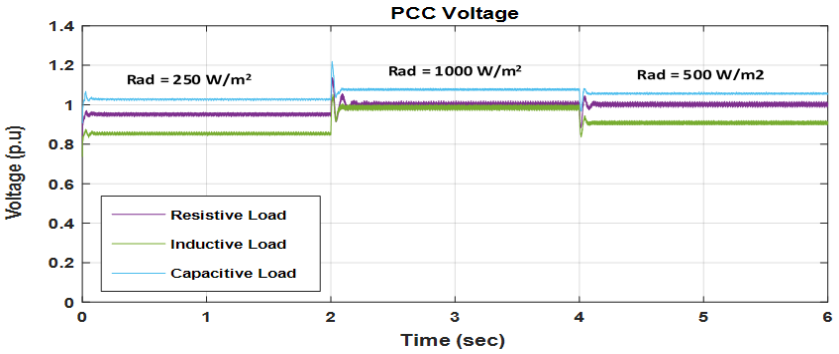

Fig. 23. The voltage at PCC for different loads with dynamic Volt-VAR control at fixed PF.

Figures 24 provide the d-q synchronous reference frame controlled currents that are responsible for controlling reactive power of the inverter, for the 33-bus test system. It is noted that in Q generation mode, *Iq* has a value related to the dynamic voltage regulation at PCC and is limited to the reactive power capability of the PV inverter. Figure 25 shows the reactive power flow over the distribution system in the case of reactive power compensation of the PV inverter. The PV inverter provides a portion of the reactive power compensation throughout the distribution network. The amount of supplied reactive power increases with the increase in solar radiation as the PV array output power increases.

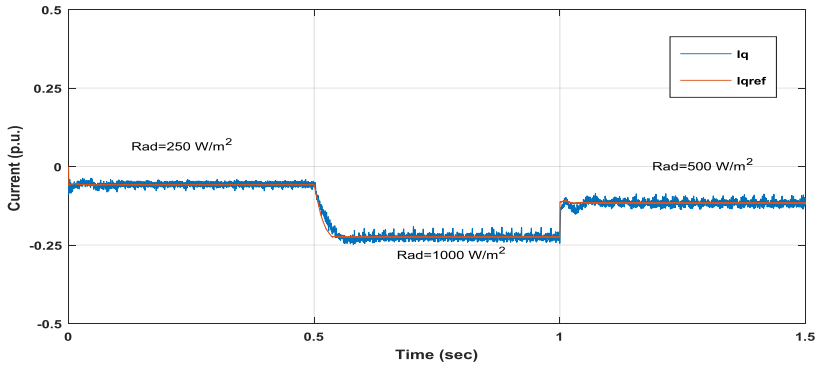

Fig. 24. Actual and reference quadrature control currents at Volt-VAR control.

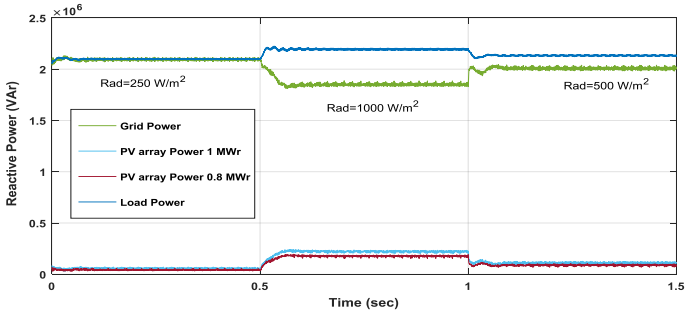

Fig. 25. Reactive PV array output power, load power, and grid power at Volt-VAR control for the 33-bus system.

Figure 26 represents the voltage profile of the 33-bus system at different radiation levels and consequently different power levels output from the PV array. This figure is represented for the two laterals at which the PV array generation units are connected. Lateral number 1 is for buses from 1 to 18 (PV array placed at bus 14; Figure 26. a) while lateral number 2 is for buses from 26 to 33 (PV array placed at bus 30; Figure 26. b). It can be noted that as the output power increase, the voltage profile values increase and improve the voltage level within the permissible grid limits. Similarly, the active power losses improve (gaining more reduction) with the radiation increase as given in Figure 27.

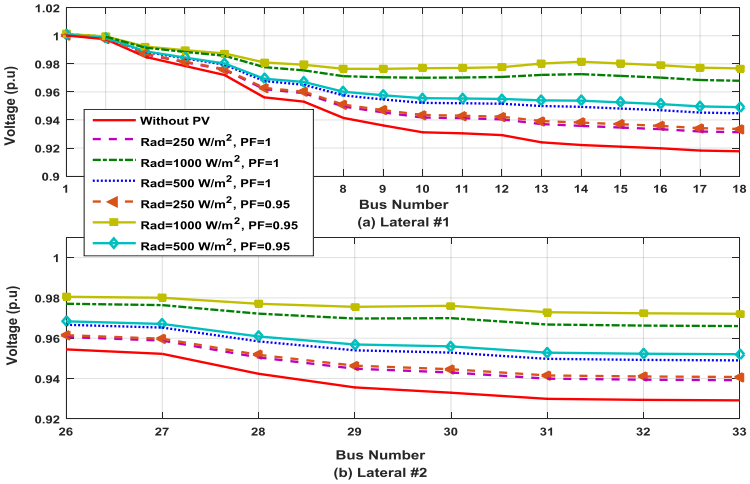

Fig. 26. Voltage profile for the 33-bus system.

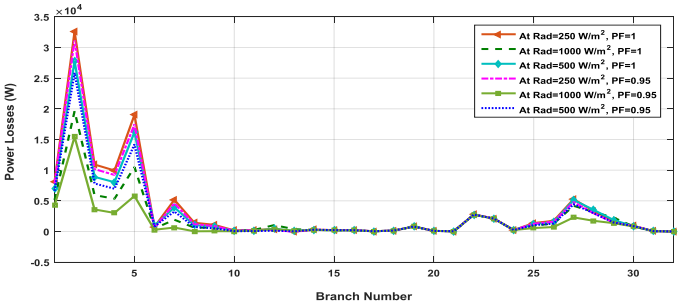

Fig. 27. Active power losses of the 33-bus system at different radiation levels.

5. Conclusion

The PV inverters are usually set to operate at a unity power factor. So, the PV arrays only supply active power to the utility grid. In this paper, a dynamic control methodology was proposed for reactive power control of PV inverters. As a result, the PV generators can be used as a controlled reactive power source which is a requirement for future smart power grids. The proposed smart PV inverter control technique has been performed to achieve two control objectives which are the maximum power point tracking (MPPT) control and the active/reactive power control. The MPPT control is used to deliver the maximum PV array power to the grid. The power control is designed to regulate the voltage and the reactive power injected into the grid. The optimized Volt-VAR control strategy is used to determine how much reactive power should be injected into the grid corresponding to the output real power, the output voltage and at the same time following the IEEE standards for the

reactive power capability of PV inverters. Adaptive GA optimization methodology is used to optimize the proposed controllers' parameters. A robust MPPT technique using fuzzy logic was proposed which is suitable for single-stage PV inverters. The results showed that the FLC-based MPPT outputs a stable reference DC voltage with minor oscillations suitable for grid integration and Volt-VAR control capability of PV inverters. The active – reactive decoupled control of PV inverters was performed for unity power factor and Volt-VAR compensation. The GA optimization of the PI controllers' parameters has been proven good performance under varying solar radiation. The proposed control technique was then tested to a 33-bus radial distribution system using their dynamic models in MATLAB/SimPowerSystem environment to validate the proposed control methodology and to show the interactions between the tested distribution network and the multiple renewable PV-DG systems with its proposed control methodology. The results prove that the proposed PCC Volt-VAR controllers lead to effective and robust PCC voltage regulation using PV systems with both active and reactive power. Further, the proposed operation strategies enabled the effective utilization of PV power to contribute to grid voltage control. The proposed control strategy in this work is also robust to consider different topologies of distribution networks with multiple PV-DG sources.

References

[1] S. Adhikari and F. Li, "Coordinated V-f and P-Q control of solar photovoltaic generators with MPPT and battery storage in microgrids," *IEEE Trans. Smart Grid*, vol. 5, no. 3, pp. 1270–1281, 2014, doi: 10.1109/TSG.2014.2301157.

[2] F. L. and P. I. H. Li, Y. Xu, S. Adhikari, D. T. Rizy, "Real and reactive power control of a three-phase single-stage PV system and PV voltage stability," in *IEEE Power and Energy Society General Meeting*, 2012, pp. 1–8. doi: 10.1109/PESGM.2012.6343965.

[3] M. F. Ansari, S. Chatterji, and A. Iqbal, "Fuzzy logic-based MPPT controllers for three-phase grid-connected inverters," *Int. J. Sustain. Energy*, vol. 32, no. 3, pp. 186–195, 2013, doi: 10.1080/14786451.2011.605948.

[4] B. S. and K. Y. L. Y. Kim, H. Cha, "Design and control of a grid-connected three-phase 3-level NPC inverter for Building Integrated Photovoltaic systems," in *2012 IEEE PES Innovative Smart Grid Technologies, ISGT 2012*, 2012, pp. 1–7. doi: 10.1109/ISGT.2012.6175663.

[5] S. Ozdemir, N. Altin, and I. Sefa, "Single stage three level grid interactive MPPT inverter for PV systems," *Energy Convers. Manag.*, vol. 80, pp. 561–572, Apr. 2014, doi: 10.1016/J.ENCONMAN.2014.01.048.

[6] M. JUAMPEREZ, G. YANG, and S. B. KJÆR, "Voltage regulation in LV grids by coordinated volt-var control strategies," *J. Mod. Power Syst. Clean Energy*, vol. 2, no. 4, pp. 319–328, Jan. 2014, doi: 10.1007/S40565-014-0072-0/FIGURES/16.

[7] S. Adhikari, F. Li, and H. Li, "P-Q and P-V Control of Photovoltaic Generators in Distribution Systems," *IEEE Trans. Smart Grid*, vol. 6, no. 6, pp. 2929–2941, Nov. 2015, doi: 10.1109/TSG.2015.2429597.

[8] S. I. Nanou, A. G. Papakonstantinou, and S. A. Papathanassiou, "A generic model of two-stage grid-connected PV systems with primary frequency response and inertia emulation," *Electr. Power Syst. Res.*, vol. 127, pp. 186–196, Oct. 2015, doi: 10.1016/J.EPSR.2015.06.011.

[9] Y. A. I. Mohamed and E. F. El-Saadany, "Adaptive decentralized droop controller to preserve power sharing stability of paralleled inverters in distributed generation microgrids," *IEEE Trans. Power Electron.*, vol. 23, no. 6, pp. 2806–2816, 2008, doi: 10.1109/TPEL.2008.2005100.

[10] X. Su, M. A. S. Masoum, and P. J. Wolfs, "Optimal PV inverter reactive power control and real power curtailment to improve performance of unbalanced four-wire LV distribution networks," *IEEE Trans. Sustain. Energy*, vol. 5, no. 3, pp. 967–977, 2014, doi: 10.1109/TSTE.2014.2313862.

[11] G. Kerber, R. Witzmann, and H. Sappl, "Voltage limitation by autonomous reactive power control of grid connected photovoltaic inverters," in *CPE 2009 - 6th International Conference-Workshop - Compatability and Power Electronics*, 2009, pp. 129–133. doi: 10.1109/CPE.2009.5156024.

[12] E. M. Khawla, D. E. Chariag, and L. Sbita, "A control strategy for a three-phase grid connected pv system under grid faults," *Electronics*, vol. 8, no. 8, pp. 1–16, 2019, doi: 10.3390/electronics8080906.

[13] M. J. Mnati, D. V. Bozalakov, and A. V. den Bossche, "PID Control of a Three Phase Photovoltaic Inverter Tied to a Grid Based on a 120-Degree Bus Clamp PWM," *IFAC-PapersOnLine*, vol. 51, no. 4, pp. 388–393, Jan. 2018, doi: 10.1016/J.IFACOL.2018.06.097.

[14] A. Ellis *et al.*, "Reactive Power Interconnection Requirements for PV and Wind Plants-Recommendations to NERC," 2012. Accessed: Mar. 18, 2022. [Online]. Available:

http://www.ntis.gov/help/ordermethods.asp?loc=7-4-0#online

[15] A. A. Hassan, F. H. Fahmy, A. A. Nafeh, and M. A. Abu-elmagd, "Genetic single objective optimisation for sizing and allocation of renewable DG systems," *Int. J. Sustain. Energy* , vol. 36, no. 6, pp. 545–562, Jul. 2015, doi: 10.1080/14786451.2015.1053393.

[16] S. Sezen, A. Aktas, M. Ucar, and E. Ozdemir, "A three-phase three-level NPC inverter based grid-connected photovoltaic system with active power filtering," in *16th International Power Electronics and Motion Control Conference and Exposition, PEMC 2014*, Dec. 2014, pp. 1331–1335. doi: 10.1109/EPEPEMC.2014.6980697.

[17] A. A. Hassan, E. M. Abdallah, M. I. Elsayed, and M. M. Elgazzer, "Coyote multi-objective optimization algorithm for optimal location and sizing of renewable distributed generators," *Int. J. Electr. Comput. Eng.*, vol. 11, no. 2, pp. 975–983, 2021, doi: 10.11591/ijece.v11i2.pp975-983.

[18] M. E. Baran and F. F. Wu, "Network reconfiguration in distribution systems for loss reduction and load balancing," *IEEE Trans. Power Deliv.*, vol. 4, no. 2, pp. 1401–1407, 1989, doi: 10.1109/61.25627.

[19] T. Ostrem, W. Sulkowski, L. E. Norum, and C. Wang, "Grid connected photovoltaic (PV) inverter with robust phase-locked loop (PLL)," in *2006 IEEE PES Transmission and Distribution Conference and Exposition: Latin America, TDC'06*, 2006, pp. 1–7. doi: 10.1109/TDCLA.2006.311434.

[20] F. Lasnier and T. Gan Ang, *Photovoltaic engineering handbook*. New York: CRC Press, 1990. doi: 10.1201/9780203743393/PHOTOVOLTAIC-ENGINEERING-HANDBOOK-FRANCE-LASNIER-TONY-GAN-ANG.

[21] A. A. Hassan, F. H. Fahmy, A. A. Nafeh, and M. A. El-Sayed, "Modeling and Simulation of a Single Phase Grid Connected Photovoltaic System," *WSEAS Trans. Syst. Control*, vol. 5, no. 1, pp. 16–25, 2010.

[22] E. Koutroulis and F. Blaabjerg, "Overview of Maximum Power Point Tracking Techniques for Photovoltaic Energy Production Systems," *Electr. Power Components Syst.*, vol. 43, no. 12, pp. 1329–1351, Jul. 2015, doi: 10.1080/15325008.2015.1030517.

[23] P. Mohanty, G. Bhuvaneswari, R. Balasubramanian, and N. K. Dhaliwal, "MATLAB based modeling to study the performance of different MPPT techniques used for solar PV system under various operating conditions," *Renew. Sustain. Energy Rev.*, vol. 38, pp. 581–593, Oct. 2014, doi: 10.1016/J.RSER.2014.06.001.

[24] B. Subudhi and R. Pradhan, "A comparative study on maximum power point tracking techniques for photovoltaic power systems," *IEEE Trans. Sustain. Energy*, vol. 4, no. 1, pp. 89–98, 2013, doi: 10.1109/TSTE.2012.2202294.

[25] J. Martinez-Nolasco, V. Samano-Ortega, E. Rodriguez-Segura, R. Orozco-Guerrero, and M. Santoyo-Mora, "Implementation of an Embedded Control for the Maximum Power Point Tracker in Photovoltaic systems," *J. Electr. Syst.*, vol. 17, no. 4, pp. 389–406, 2021.

[26] F. H. M. Rafi, M. J. Hossain, and J. Lu, "Design of a single stage transformerless VSI in a smart microgrid for PV-STATCOM/ESS operations," in *2014 Australasian Universities Power Engineering Conference, AUPEC 2014 - Proceedings*, Nov. 2014, pp. 1–6. doi: 10.1109/AUPEC.2014.6966557.

[27] A. Ellis *et al.*, "Reactive power performance requirements for wind and solar plants," in *IEEE Power and Energy Society General Meeting*, 2012, pp. 1–8. doi: 10.1109/PESGM.2012.6345568.

[28] D. Jose, "Comparison of a three phase single stage PV system in PSCAD and PowerFactory," KTH Electrical Engineering, Sweden, 2012. Accessed: Mar. 18, 2022. [Online]. Available: https://energynautics.com/content/uploads/2019/02/App12_KTH_Master_Thesis_Comparison_of_a_three_phase_single_stage_PV_system_in_PSCAD_-and_PowerFactory.pdf

[29] I. Pisică, P. Postolache, and M. M. Edvall, "Optimal Planning of Distributed Generation via Nonlinear Optimization and Genetic Algorithms," in *Handbook of Power Systems I*, Springer, Berlin, Heidelberg, 2010, pp. 451–482. doi: 10.1007/978-3-642-02493-1_20.

[30] F. G. Martins, "Tuning PID Controllers using the ITAE Criterion," *Int. J. Eng. Educ.*, vol. 21, no. 5, pp. 867–873, 2005.

[31] A. A. Hassan, F. H. Fahmy, A. A. Nafeh, and M. A. Abu-elmagd, "Hybrid genetic multi objective/fuzzy algorithm for optimal sizing and allocation of renewable DG systems," *Int. Trans. Electr. Energy Syst.*, vol. 26, no. 12, pp. 2588–2617, Dec. 2016, doi: 10.1002/ETEP.2223.